



International Journal of Intellectual Advancements and Research in Engineering Computations

Current status of micro and nano structured optical fiber sensors

R.Nagaraju¹, Dr. S. Venkateswara Rao²

¹Department of Physics, Holy Mary Institute of Technology & Science Engineering College,
Hyderabad, Telangana-501301 (India).

²Department of Physics, JNTUH College of Engineering (Autonomous), Hyderabad, Telangana-
500072 (India).

ABSTRACT

Recently developed micro- and Nano-structured optical fiber sensors, with particular reference to surface Plasmon resonance (SPR) fiber sensors and photonic crystal fiber (PCF) sensors are reviewed; SPR fiber sensors can have diverse structures such as D-shape, cladding-off, fiber tip structures. Also reviewed the recently developed novel structures include the use of various types of fiber gratings in SPR fiber sensors. PCF sensors cover diverse recent developments on photonic-bandgap fiber, holey fiber, hole- assisted fiber and Bragg fiber sensors. Major applications of these include gas sensors and biosensors. These micro and Nano structured fiber sensors have attracted considerable research and development interest, because of their distinct advantages, which include high sensitivity, small sensor head footprint and the flexibility of the optical fibers.

INTRODUCTION

Optical fiber sensors have a long history of research [1]. As a result, many types of fiber sensor technologies are currently approaching saturation, from the standpoint of research and some have already been commercialized. However, with the recent remarkable progress in surface Plasmon resonance (SPR) and photonic crystal fiber (PCF) technologies, new types of fiber sensors, i.e., micro and Nano structured fiber sensors, have attracted the attention of researchers. It is not possible to review the entire body of information in this area, given the limitations on the length of a paper such as this, and some excellent reviews on some of the topics have already appeared [2]. In this review, we will discuss the key concepts of such fiber sensors and review some of the more recent results, with emphasis on SPR fiber sensors and PCF sensors.

Surface Plasmon resonance optical fiber sensors:

The development of fiber-optic SPR sensors began in the early nineties of the last century.

Although a paper proposing fiber coupling for SPR sensors appeared in 1990 [3], real fiber SPR sensors that use fiber devices as sensor heads were first proposed in 1993 [4]. Since that time, optical fiber SPR sensor has been a subject of continuous research. The SPR fiber sensor has the capacity to detect changes in external refractive index. It can be optimized by adjusting parameters such as the thickness of the metal layer and over layer, etc. [5]. Several theoretical as well as experimental studies have been carried out, in attempts to improve the performance of fiber-optic SPR sensors.

PRINCIPLE OF SURFACE PLASMON RESONANCE FIBER SENSORS

SPR refers to the excitation of surface Plasmon polaritons (SPPs), which are electromagnetic waves coupled with free electron density oscillations on the surface between a metal and a dielectric medium (or air). SPPs or surface

Author for correspondence:

Department of Physics, Holy Mary Institute of Technology & Science Engineering College, Hyderabad,
Telangana-501301 (India)

plasmon waves (SPWs) propagate along the interface of the metal and dielectric material as shown in Figs. 1(a) and (b). For nano-scaled metallic structures such as metallic nano-particles, islands or rods, a light with the appropriate wavelength can be used to excite the localized oscillation of charges as shown in Fig. 1(b), a process that is referred to as localized surface plasmon resonance (LSPR). SPR techniques excite and detect collective oscillations of free electrons (known as surface plasmons) via the Kretschmann's configuration, in which light is focused onto a metal film through a glass prism and the subsequent reflection is detected.

As shown in Fig. 1(a), because of the presence of the surface normal electric field component,

only a TM wave can excite SPR. An important feature of SPPs is that the field amplitudes are at a maximum at the interface between the metal and dielectric medium and decays exponentially on both sides of the material, as shown in Fig. 1(b). This unique characteristic can be attributed to the fact that metals such as gold, silver, copper and aluminum have a negative electric permittivity (complex, in fact. Its real part is negative.) for light, while dielectric media have a positive electric permittivity. Among the numerous possible metals that can be used, silver, which has the sharpest SPR resonance peak and gold, which shows excellent surface stability are commonly employed.

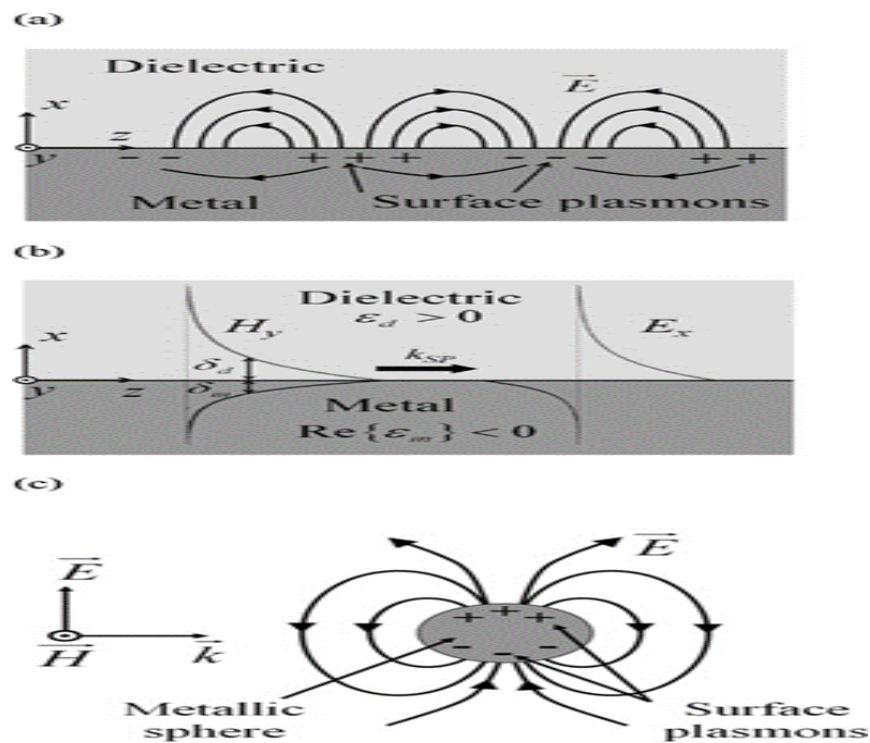


Fig.1. (a) Surface plasmon polariton (SPP) propagating along the interface between the dielectric with the permittivity ϵ_d and the metal with the permittivity of ϵ_m .

Field distribution of the SPP. E_z has a similar profile to H_y . The penetration depths to the dielectric and the metal are denoted by δ_d and δ_m , respectively.

Schematic diagram of the localized surface plasmon resonance in a metallic sphere.

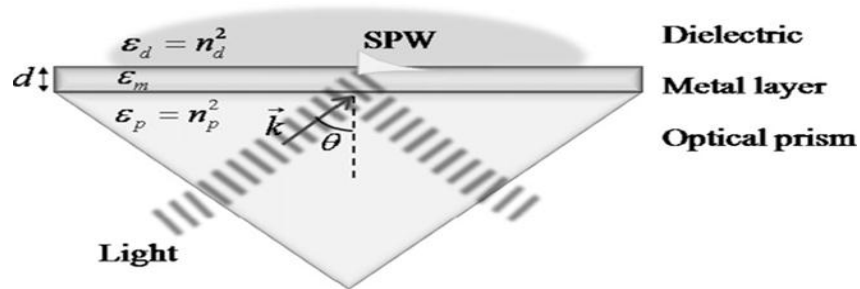


Fig.2. Kretschmann's schematics for the excitation of surface plasmons using the attenuated total reflection method.

There are several methods available for exciting SPR including prism coupling, waveguide coupling, fiber-optic coupling, and grating coupling. The most common approach to exciting SPWs is the attenuated total reflection method by means of a prism coupler, which is referred to as the Kretschmann's method [12]. In this method, a high refractive index prism with refractive index n_p is coated with a thin metal film with permittivity ϵ_m and thickness d , and a semi-infinite dielectric with refractive index n_d ($n_d < n_p$) is positioned outside it, as shown in Fig. 2. When a

light propagating in the prism is incident on the metal film with an angle larger than the critical angle formed by the relation of n_p and n_d , it is basically reflected back into the prism. Evanescently decaying fields penetrate into the metal layer, and, because the metal thickness is thin (< 100 nm), fields remain at the other boundary. (Between metal and n_d medium). Under a phase matching condition, this may excite SPWs at the boundary, and the SPWs then propagate along the boundary.

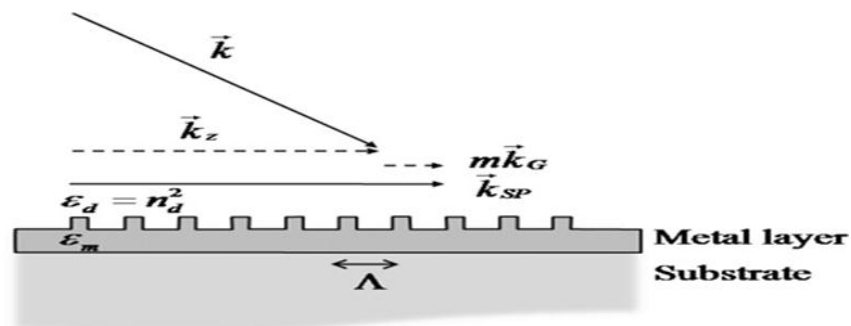


Fig.3. Excitation of surface plasmons by a surface grating, $k_G = 2\pi / \Lambda$.

The propagation constant of SPWs, k_{SP} , propagating along the interface of the metal film and the dielectric (M/D), is influenced by the presence of the dielectric on the opposite side of the metal film, i.e. by n_d , and can be expressed as

$$k_{SP} = \text{Re} \left(\frac{2\pi}{\lambda} \sqrt{\frac{\epsilon_d \epsilon_m}{\epsilon_d + \epsilon_m}} \right) \quad (1)$$

Where $\epsilon_d = n_d^2$ and ϵ_m are the permittivities of the dielectric medium and metal, respectively, and λ is the wavelength of light in a vacuum. The propagation constant k_z for evanescent wave along the interface of metal and prism (M/P) is given by

$$k_z = \frac{2\pi}{\lambda} n_p \sin \theta, \quad (2)$$

Where θ is the incidence angle of light as shown in Fig. 2. If k_z matches k_{SP} , i.e., if Eqs. (1) and (2) are equal, SPWs become excited. Note that no SPW exists at the M/P interface. SPWs may only exist at the M/D interface in this case of $n_d < n_p$. The evanescent wave penetrating through the metal may induce SPP excitations at the M/D interface, which radiate light back into the metal film and the radiation destructively interferes with

the reflected component of the incident light and hence, leads to a reduction in the overall reflection, if the thickness of the metal film is thin. In an ideal case, the overall reflection becomes zero and the entire radiation field is converted to SPWs at the M/D interface. In general insulator-metal-insulator structures, the existence of symmetric and antisymmetric SPP modes is possible. However, in the case of the Kretschmann's excitation method, those modes cannot be excited. An SPW can also be excited by gratings on a metal surface, as shown in Fig. 3. If the wave vector of light diffracted by the surface grating is parallel to the grating surface and is the same as the propagation constant of the SPPs, the light will be coupled into the SPW, as described in the equation below:

$$\frac{2\pi}{\lambda} n_d \sin \theta + m \frac{2\pi}{\Lambda} = \pm k_{sp}, \quad (3)$$

Where m is an integer representing the diffraction order and Λ is the grating period. However, with the grating coupling, the incident light directly illuminates the metal surface. Because of this, the sample layer or sample fluid must be optically transparent, in order for light to pass through it. This method can be used in reverse; that is, SPWs can be converted into light by a grating. Optical fiber SPR sensors are basically similar to the Kretschmann's prism structure, where the prism is replaced with a fiber core, as shown in Fig. 4. The figure shows the fundamental structure of an SPR fiber sensor, in which the cladding has been etched off and core is symmetrically coated with metal. Optical fibers can excite the SPW in an easy and flexible manner. From Eqs. (1) and (2) we obtain

$$\frac{2\pi}{\lambda} n_{fiber} \sin \theta = \text{Re} \left(\frac{2\pi}{\lambda} \sqrt{\frac{\epsilon_s \epsilon_m}{\epsilon_s + \epsilon_m}} \right), \quad (4)$$

Where, n_{fiber} is the fiber core refractive index and ϵ_s is the dielectric function (permittivity) of the superstrate material (sample medium) in Fig. 4. Since SPWs are on the boundary between the metal and the sample medium, their excitation condition is very sensitive to any change in boundary condition such as the adsorption of molecules to the metal surface. A change in the refractive index in the superstrate (sample medium) produces a change in the propagation constant of the SPW. This change alters the coupling condition between a light wave and the SPPs, which can be observed as a change in the characteristics of the optical wave that interacts with SPWs. In Eq. (4) the change in ϵ_s results in a change in the angle or wavelength for an SPR. When the values of the angle and wavelength are fixed, the change in ϵ_s results in a change in the intensity of the reflected light (or light intensity guided by optical fiber) due to the violation of the phase-matching condition of Eq. (4). In general, SPR sensors with resonance angle monitoring or resonance wavelength monitoring, as in Fig. 5, are in the most widespread use. As pointed out in the above, the optical fields of SPWs are at a maximum at the interface and decay on both sides of metal and dielectric (sample region). The depth of penetration (defined as the depth for which the field is decreased by $\exp(-1)$ compared with the field at the interface) through a dielectric medium can be represented as

$$\delta_d = \left[\text{Re} \left(j \frac{2\pi}{\lambda} \frac{\epsilon_d}{\sqrt{\epsilon_m + \epsilon_d}} \right) \right]^{-1}. \quad (5)$$

Table 1 Refractive indexes of typical materials used in plasmonic, the propagation length (L_p) and the penetration depth to the dielectric (δ_d) and the metal (δ_m).

@ 633 nm			@ 1550 nm		
Metal Dielectric	Silver (0.135 + i3.99)	Gold (0.197 + i3.09)	Metal Dielectric	Silver (0.469 + i9.32)	Gold (0.559 + i9.81)
Air (1.00)	L_p : 22 μm δ_d : 390 nm δ_m : 24 nm	6.5 μm 290 nm 31 nm	Air (1.00)	215 μm 2.3 μm 38 nm	215 μm 2.4 μm 25 nm
Water (1.33)	8.5 μm 210 nm 24 nm	2.4 μm 160 nm 29 nm	Water (1.32)	90 μm 1.3 μm 26 nm	89 μm 1.4 μm 25 nm
SiO2 (1.54)	5.1 μm 160 nm 23 nm	1.4 μm 110 nm 28 nm	SiO2 (1.53)	57 μm 0.97 μm 26 nm	56 μm 1.0 μm 25 nm

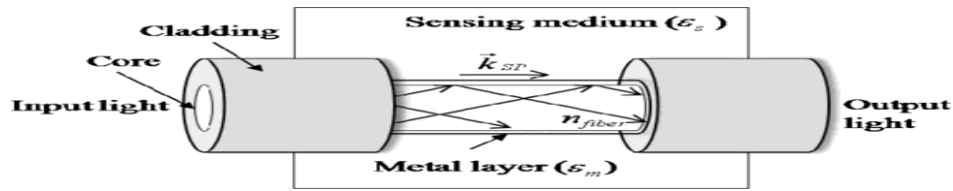


Fig.4. Basic structure of an optical fiber surface plasmon resonance sensor.

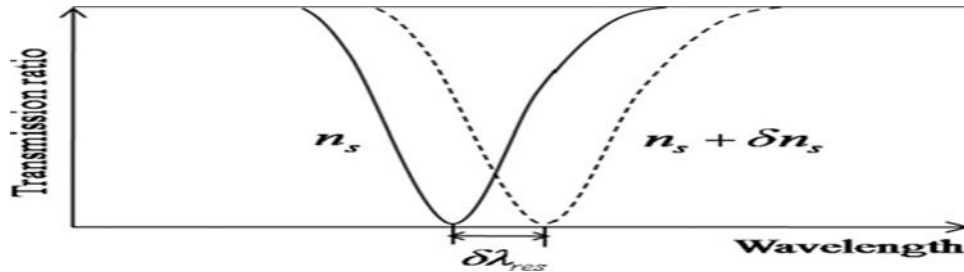


Fig. 5. Transmission ratio of light after interacting with surface plasmon polaritons as a function of wavelength for two different refractive indexes of sensing medium.

Table 1 shows penetration depths and permittivities for several wavelengths metals and dielectrics. The SPR sensor has several advantages compared to other types of conventional sensors. First, the SPR sensor head provides very high sensitivity, several times faster response (actual speed is determined by the use of a demodulation (i.e., monitoring) system), and the size of the sensing region is smaller. (The typical propagation length of an SPW is in the order of μm .) In addition, SPR sensors, especially metal nanoparticle sensors, simultaneously exhibit an LSPR effect and surface-enhanced Raman scattering (SERS). As a result, the detection of binding events and analytes identification, even at single molecule level, in biological studies is possible with SERS [8]. Although the prism-based SPR sensor is the most convenient SPR configuration, it is somewhat bulky and contains a variety of optical and mechanical parts, which makes it difficult to optimize and commercialize the system and to construct remote sensing systems on a large scale. Miniaturization of an SPR sensor system can be achieved by the use of optical fibers. One of the important advantages of using an optical fiber is its small diameter, which allows it to be used in a very small volume. Other advantages of fiber-optic SPR sensing configurations are the simplified

optical design and the capability for remote sensing [9].

However, the SPR fiber sensor also has some drawbacks. Unlike the prism-based sensor, the angle of the incident light cannot be controlled, which makes the resonance curve in the transmission spectrum broader, resulting in a decreased sensitivity and detection limit. The use of a single mode fiber (SMF) instead of a multimode fiber (MMF) improves the characteristics of the sensor. Another barrier is that it is difficult to perform a theoretical analysis of an SPR fiber sensor. The planar structure approximation or ideal cylindrical symmetry assumption has been used in analytic approaches [10]. Of course, a full three-dimensional numerical analysis can be done. However, this is time consuming obtaining a physical insight using the method is not a straight forward task. Different from prism-based SPR measurements, which typically use a monochromatic light source while the incidence angle is modulated, the SPR fiber sensor can employ a white light source, which has a wide spectrum range, to monitor the resonance wavelength. The incident angle in a fiber is limited to the totally reflected angle of the core-cladding interface. Although a monochromatic light can be used and its transmission intensity through an optical fiber can be monitored, if a

wideband light is used, it becomes possible to monitor resonance wavelength variation in the transmitted spectral intensity distribution. As the sensing principle based on Eq. (4), a sharp dip at the resonance wavelength λ_{res} (λ in Eq. (4)) in the transmitted power spectrum is observed as in Fig. 5. The resonance wavelength shifts when the refractive index of the sensing region is represented as

$n_s = \sqrt{\epsilon_s}$ is varied. In other words, if the refractive index of the sensing region is altered by δn_s , the resonance wavelength shifts by $\delta \lambda_{res}$. The sensitivity S of SPR sensors can be defined as [11].

$$S = \frac{\delta \lambda_{res}}{\delta n_s} \quad (6)$$

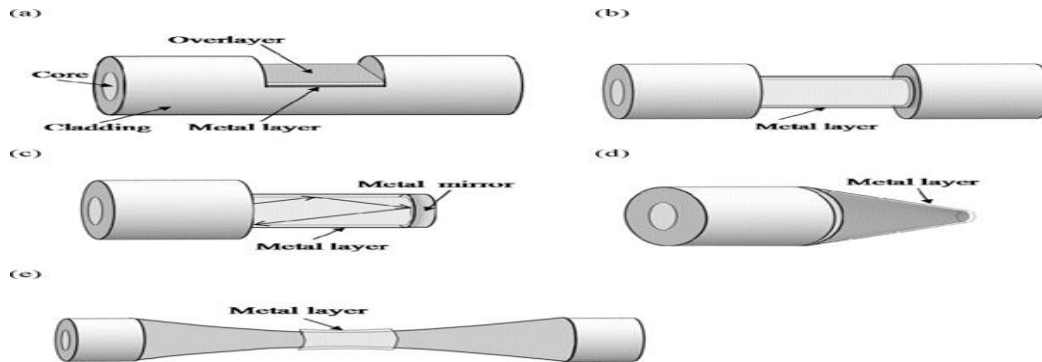


Fig. 6. General SPR fiber-optic sensor schematics with (a) D-shape fiber, (b) cladding-off fiber, (c) end-reflection mirror, (d) angled fiber tip, and (e) tapered fiber.

To calculate the sensitivity, λ_{res} can be plotted as a function of n_s , the slope of which gives the sensitivity of the sensor. The accuracy of the detection of the SPR resonance wavelength λ_{res} is dependent on the width of the response curve in the transmitted power spectrum. This indicates that a narrower width corresponds to higher detection accuracy. Below, we examine the parameters that affect the characteristics of SPR fiber sensors. First, various fundamental SPR fiber sensor configurations exist, as shown in Fig. 6 and Table 2. These include symmetrical structures, such as a simple metal coated optical fiber with and without remaining cladding [11–12], tapered fiber [13], structures without any symmetry, such as side-polished fibers (or D-shape fiber) and one-side metal coated fibers with and without remaining cladding [14], and structures with modified fiber tips with flat or angled structures [15]. Each of them may contain either overlayer or multilayer structures. The overlayer, which is a layer deposited on the metal layer, can be useful in tuning the measurable range for a fiber-optic SPR sensor. Many SPR fiber sensor systems have also

been developed with structures that have been further modified, via the use of several types of gratings, hetero core fibers, nano holes, and so on. Surface Plasmon Resonance. SPR is defined as collective oscillation of conduction electrons at the surface of the metal nanoparticles due to excitation by the corresponding resonant wavelength of light. Surface plasmon in most cases, gold is used because it gives a SPR signal at convenient combinations of reflectance angle and wavelength. The incident light photons are absorbed and the energy is transferred to the electrons, which convert into surface plasmons. In physics, a plasmon is a quantum of plasma oscillation. Thus, plasmons are collective (a discrete number) oscillations of the free electron gas density. For example, at optical frequencies, plasmons can couple with a photon to create another quasi particle called a plasmon polariton. Plasmonic nanoparticles are particles whose electron density can couple with electromagnetic radiation of wavelengths that are far larger than the particle due to the nature of the dielectric-metal interface between the medium and the particles:

unlike in a pure metal where there is maximum limit on what size An SPR sensor with MMF is generally sensitive to mechanical disturbance; hence the intensity of the output light may fluctuate with time. However, relatively simple detection electronics and a good signal-to-noise ratio are typical, because of the abundant light power at the detector. In addition, such a device is appropriate for measuring over a wide refractive index range. A sensor with SMF generally has a narrower resonance wavelength dip in the transmission spectrum than that with MMF and hence has good sensitivity. The SPR fiber sensor with a modified fiber tip is usually used as a reflection-based localized SPR fiber-optic probe, while other types of SPR fiber sensors are transmission-based sensors. To develop the SPR fiber sensor, we first need to have access to evanescent waves guided near the boundary of the core and cladding in the fiber. For this purpose, the fiber cladding can be completely or partially removed by chemical fetching, precise flame controlling, or polishing. An alternative that uses evanescent waves is tapering a fiber, which is prepared by stretching the fiber while it is heated

with the flame touch. The method used for tapering fibers is particularly well described in Ref. After exposing (or almost exposing) the fiber core region, a metal film needs to be placed on the bare (or almost bared) core region. The metallic layer can be made by depositing thermally evaporated metal or by using nano-particles that are chemically immobilized to either a colloidal suspension or a nano-particle film. For SPR sensors, the metal layer is usually deposited by evaporation. However, many novel sensors based on the LSPR spectrum of nano-particles have also been developed. As mentioned above; the metallic layer used in SPR sensor system is usually either silver or gold. Gold demonstrates a high shift in resonance parameters in response to a change in the refractive index of the sensing layer and chemically very stable. Silver displays a narrow resonance curve in the transmission spectrum, causing a high resolution in the SPR sensor, but is unstable in the presence of air and especially, water. Therefore, to prepare a reliable sensor for practical applications by silver, treatment of its surface must result in a thin and dense over layer.

Table 2: Characteristics of general SPR based fiber optic sensors

Optical structure	Characteristics	Detection RI range	Wavelength	Sensitivity	
Cladding-off cylindrical fiber	• Single metal coating	MMF, Au-Ag alloy nanoparticle	400 ~ 800 nm	~3000 nm/RIU	
		MMF, Au, surface roughness	550 ~ 1000 nm	1600 ~ 3000 nm/RIU	
		MMF, parameter analysis	400 ~ 850 nm	2266.7 ~ 2780.1 nm/RIU	
		MMF, Au	670 nm	2.5×10^{-4} RIU (intensity)	
	• Multi-metal coating	Au, Ag double layer, Au-Ag alloy nanoparticle			~2500 ~ 3000 nm/RIU
• With multi-layer	MMF, Au, dielectric multilayer (SiO ₂ , TiO ₂)	1.333 and 1.336, 1 ~ 1.313	450 ~ 950 nm	10^{-5} RIU	
Tapered fiber	• Off cladding	MMF, Au, tapering ratio	600 ~ 900 nm	2700 ~ 4900 nm/RIU	
		MMF, Au,	580 ~ 700 nm	2750 ~ 15000 nm/RIU	
	• With cladding	SMF, Au, semi-cylindrical, multiple peaks	1.444 ~ 1.454	900 ~ 1600 nm	7×10^{-7} RIU
D-shape fiber	• Single metal coating	SMF, half of core polished, Au	632.8 nm	8×10^{-5} RIU (intensity)	
		SMF, Au	750 ~ 910 nm	5000 nm/RIU	
	• With overlayer	SMF, half of core polished, Au, SiO ₂ overlayer	1.33 ~ 1.40	632.8 nm	2.5×10^{-6} RIU (phase)
		SMF, half of core polished, Au, SiO ₂ overlayer	1.33 ~ 1.40	632.8 nm	2.5×10^{-5} RIU (intensity)
		SMF, remained thin clad, Au, Ta ₂ O ₅ overlayer	1.329 ~ 1.353	750 ~ 950 nm	5×10^{-7} RIU
		SMF, Au, Al mirror, Ta ₂ O ₅ overlayer	1.328 ~ 1.338	825 nm	4×10^{-5} RIU (intensity)
	• With thin cladding	SMF, Ag, SiO overlayer	1.33 ~ 1.45	780 nm	
		PMF, polarization alignment	1.33 ~ 1.3385	770 ~ 880 nm	4×10^{-6} RIU
Modified fiber end	• Flat fiber tip	MMF, Ag end mirror, Au coating thickness	400 ~ 840 nm	1557 nm/RIU	
		MMF, Ag end mirror, Ag coating, SiO layer	650 ~ 1000 nm	3800 nm/RIU, 1000 nm/RIU	
		MMF, Ag end mirror, Au, Ag coating	400 ~ 900 nm	$5 \times 10^{-4} \sim 10^{-5}$ RIU	
	• Angled fiber tip	SMF, tapered tip	1.33 ~ 1.375	650 nm	4000%/RIU (intensity)

For the design and analysis of the sensor responses, the values for the electric permittivity of the metal films are needed. These values depend

on wavelength of light. In many SPR sensors the wavelength range covers from about 400 nm to 800 nm or is in the 1500 nm region. Values for the

electric permittivity of metals can be found in Refs. [16]. The Drude model can be used for the dispersion of metals, and is given as

$$\varepsilon(\omega) = \varepsilon_{\infty} - \frac{\omega_p^2}{\omega(\omega + i\omega_d)} \quad (7)$$

Where, ε_{∞} is the high frequency dielectric function, ω_p is the bulk plasma frequency, and ω_d is the damping frequency, respectively.

For metallic nano-particle layers, ω_d needs to be modified according to size of nano-particles used (as small as 2 nm), because of the additional surface scattering:

$$\omega_d(R) = \omega_d(bulk) + \frac{v_f}{R} \quad (8)$$

Where, R is the nano-particle size and v_f is the Fermi velocity. All related parameters and coefficients are given in Table 3.

The wavelength dependent refractive index for fused silica is also needed for applications of an optical fiber at different wave-lengths. It is generally expressed according to the Sell Meier relation that can be found in references such as Ref.

Typically demonstrated SPR fiber sensors show the sensitivity of resonance wavelength shift with respect to changes in external refractive index in the range of 103 - 104 nm per refractive index unit (RIU) with gold coating, as shown in Table 2. The sensitivity and the resonance wavelength with a specific refractive index of the sensing medium can be modulated to a certain extent by changing the film material, thickness of the metal film, or the thickness of the over layer. The thickness of the metal film is an especially crucial parameter for an SPR fiber sensor. For example, in the case of a D-shape SPR fiber sensor with a gold metal film, the resonance wavelength shifts to longer wavelength and a narrower resonance dip can be obtained if the metal film thickness is increased. However, the transmitted power dip at the resonance wavelength becomes shallower. This indicates a thin metal film (<100 nm) should be used, because the evanescent field decays exponentially in the metal layer and the SPR becomes weaker with increasing thickness.

Table 3 Parameters and coefficients for the drude model of metals (Ref. [23]).

Parameters	Silver	Gold
High frequency dielectric constant, ε_{∞}	2.48	7.0
Plasma frequency, ω_p (rad/s)	1.35×10^{16}	1.40×10^{16}
Damping frequency, ω_d (rad/s)	7.62×10^{13}	3.78×10^{13}
Fermi velocity, v_f (m/s)	1.40×10^6	1.40×10^6

To produce an accurate SPR sensor, a narrow and deep resonance curve is preferred. Hence, to improve the characteristic of the sensor, it is necessary to optimize the thickness of the metal film. The film thickness of the sensor has an effect on sensitivity [17]. A deep resonance in the transmission spectrum can also be obtained by stretching the length of the sensing region. The longer length of the sensing region increases the absorption of the propagating light into the metal, which results in a deep resonance dip, and also a reduction in sensitivity. This suggests, therefore, that the sensing region of an SPR fiber sensor should be fabricated to have a smaller length in order to achieve high sensitivity and high resolution. It should also be noted that, if the thickness of the residual cladding is over than several μm , the coupling of the evanescent wave

with SPR wave is difficult, in that the resonance wavelength dip in the transmitted power spectrum becomes shallower.

An over layer, such as SiO₂ or Ta₂O₅ employed in the SPR sensor, also affects the resonance wavelength. As mentioned above, the over layer is required to protect the silver surface. On the other hand, a layer over or under the metal layer can also be used to adjust the resonance wavelength in the transmission spectrum of an SPR sensor. A structure comprised of bimetallic layers with silver and gold deposited on the optical fiber has been proposed by Sharma and Gupta [18]. This structure displayed a high shift in resonance parameter (i.e., angle or wavelength), similar to a gold film, and showed a narrower resonance curve, similar to a silver film, thus providing a high

resolution in addition to protecting silver against oxidation.

The overlayer also affects the sensing range of the refractive index. Without an overlayer, if the refractive index of the sensing region is higher than that of the core, then much of guided light leaks out of the fiber. This imposes a limitation in the sensing range of the refractive index. Hence, if a material that has higher refractive index than the core is overlaid, the sensing range of the refractive index can be changed to a higher level. The same effect can also be achieved by using a different fiber core material that has a higher refractive index than a conventional optical fiber. When one uses a nano-particle film as a metal layer, which is made by chemical immobilization to the fiber, there are more parameters to consider in SPR sensors. As pointed out earlier, the phenomenon in nano-particles is the LSPR. The absorption rate and the resonance wavelength of LSPR are highly dependent on the size and shape of the nano-particles used. The performance of core-shell nano-particle-layer-based fiber optic SPR sensor has been found to be better and faster than conventional fiber optic sensors [19-20]. A sensor using a tapered fiber requires a simple technology for its preparation and shows a better efficiency in sensing than the polished type fiber sensor [21]. In designing the sensor head, the tapering ratio and the diameter of the uniform region need to be considered. When one designs a reflection type of SPR fiber sensor with a metal-coated fiber tip, the angle and the shape of the tips should also be considered [22]. SPR resonance is also affected by environmental temperature. Hence a temperature correction is required because a temperature variation of 1 °C in an aqueous solution is associated with a change in its refractive index in the order of the detectable signal for SPR sensors [23]. Measured the temperature-related resonance wavelength change in an SPR sensor. According to their results, the resonance wavelength approximately follows a linear relationship with a negative slope with respect to increasing temperature.

To analyze the above-mentioned parameters of SPR fiber sensor structures, several methods of analysis can be used. Theoretical analyses for

cylindrical geometry have been described by a number of authors, and especially a dielectric circular cylinder coated with coaxial metallic film was described by Al-Bader. For the case of asymmetric geometry, it is difficult to obtain an analytic description because of the degeneration of SPP modes as well as geometric complexity. In addition, many SPR fiber sensors have a unique characteristic of asymmetric geometry. The transmission spectrum is greatly dependent on the polarization state of the input light. The guiding mode of the fiber that is orthogonal to the SPP mode for a symmetric structure can also excite SPP modes in an asymmetric structure since they are no longer orthogonal. Consequently, TM and TE spectra of asymmetric geometry are clearly different and TE spectra show multiple dips. Hence, to study the characteristics of the SPR fiber sensors with asymmetry geometry, a numerical analysis is needed. In most analyses, for properly modeling SPR fiber sensors with symmetric geometry or asymmetric geometry, one usually simplifies an optical fiber to one- or two-dimensional layer structures, to reduce the calculation burden. Plasmonic materials are metals or metal-like materials that exhibit negative real permittivity. Most common plasmonic materials are gold and silver. However, many other materials show metal-like optical properties in specific wavelength ranges. Plasmonic nanoparticles are particles whose electron density can couple with electromagnetic radiation of wavelengths that are far larger than the particle due to the nature of the dielectric-metal interface between the medium and the particles: unlike in a pure metal where there is a maximum limit on what size. The layered structure model was proposed early on, which substituted an optical fiber with an equivalent three-layer planar waveguide. The layered structure can be analyzed using the mode expansion and propagation method (MEP) [24-25]. For example, in the case of a curved side polished fiber, the bending effect was accounted for by substituting the bent waveguide by several sections of a straight waveguide with different lengths and distances from the metal film, as shown in Fig. 7(a).

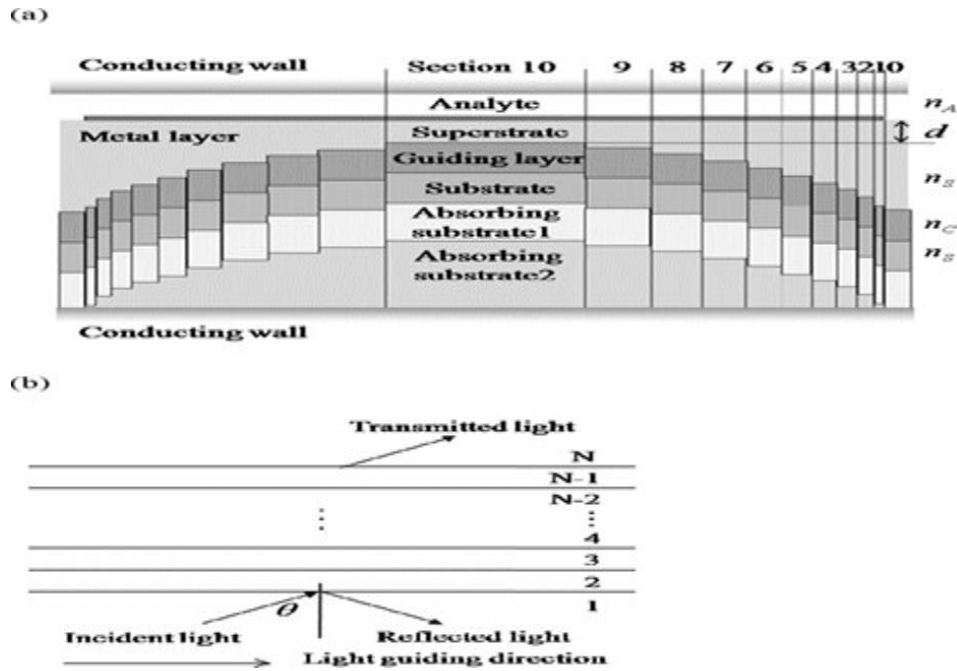


Fig. 7. Representation of the SPR fiber sensor system (a) by a multi-section planar waveguide for MEP modeling and (b) by a layered structure for transfer matrix modeling.

Another method, transfer matrix formalism for a multilayer system, can also be used for modeling. By using the transfer matrix formalism, the reflectance of the light can be computed based on the calculation of light propagation through a multilayer medium consisting of several isotropic and homogeneous layers as in Fig. 7(b). This method considers only a small portion of the fiber near the metal film and is very useful in applications to a system with any number of layers. It is very easy and the accuracy is good, due to the absence of approximations. In another method, one can theoretically investigate an SPR structure based on angle scanning by a rigorous coupled wave analysis (RCWA), which is frequently applied to grating-coupled type SPR structures [26-27]. The calculation result by each of the above mentioned methods can be employed to an optimization tool. For example, an evolution

algorithm can be employed as an optimization tool. In optimized SPR fiber sensors, the parameters mentioned above need to be considered, i.e., the thickness of the metal film, the remaining cladding thickness, the over layer, the length of the sensing region, tapering ratio, and so on. In addition, the effect of polarization-cross coupling or variations in the transmitted light phase needs to be included in some cases.

Performance of SPR fiber sensors and other recent novel structures

In the past few years, sensitivity enhancement has been an important issue in fiber SPR sensors. Several theoretical and experimental studies have been carried out, in attempts to improve the performance of sensors. Sensors with novel structures have also been proposed by many authors, as shown in Table 4.

Table 4
Performance of novel SPR based fiber-optic sensors.

Optical structure	Characteristics	Detection IR range	Wavelength	Sensitivity	
With fiber grating	• Tilted grating	SMF, angled FBG, Au, D-shape	1.30 ~ 1.38	1220 ~ 1700 nm	3365 nm/RIU
		SMF, tilted grating, Au	1.4211 ~ 1.4499	1520 ~ 1555 nm	454 nm/RIU
	• LPG	3 μ m core planar, Au	1.329 ~ 1.340	~1550 nm	1100 nm/RIU
		SMF, Au colloidal	1.33 ~ 1.39	~1520 nm	-23.45 nm/RIU
	• FBG	MMF, Au	1 ~ 1.44, 1.33		150 ~ 280 nm/RIU
	26 μ m core planar, Au	1.33 ~ 1.338	1550 ~ 1553 nm	300 nm/RIU	
Metallic grating	SMF, tapered, Au, metal surface grating,	1 ~ 1.41	1200 ~ 1500 nm	500 nm/RIU	
Two region coating	SMF, Au, temp. correction, self-referencing	1.32 ~ 1.36,	600 ~ 1400 nm	$1 \times 10^{-4} \sim 5 \times 10^{-5}$ RIU	
	MMF, Au, cascade sensing layer	1.3333 and 1.3338	500 ~ 1700 nm	2×10^{-5} RIU	
Absorption layer	Tapered fiber, silver and praseodymium oxide		450 ~ 600 nm		
Dual light source	MMF, two LEDs	1.333 ~ 1.3616	609.6 and 675.9 nm	5.2×10^{-4} RIU	
Modified fiber end	MMF, GIF, hole milling	1.33 ~ 1.376	440 ~ 760 nm	533 nm/RIU	
Photonic crystal fiber	Three hole, Au, dielectric layer	1.33 and 1.34	500 ~ 600 nm	10^{-4} RIU	
	Hollow core Bragg fiber, honey comb PCF, Au			$7 \times 10^{-6} \sim 5 \times 10^{-5}$ RIU	
	Micro-structured optical fiber, Au			10^{-4} RIU/(intensity)	

Some approaches employ various gratings to couple light from the core mode to various cladding modes and to provide the phase matching needed to excite SPR on the surface of an optical fiber, as shown in Fig. 8(a). In one, He et al. suggested an SPR fiber sensor adopting cascaded long period gratings (LPGs), in which it was theoretically shown that the propagation constant of the excited particular cladding mode can be matched with that of SPW. Tang et al. also employed LPG to SPR fiber sensor with self-assembled gold colloids on the grating portion, which is intended for use in sensing the concentration of a chemical solution and for the label free detection of bimolecular binding at a nano-particle surface [29]. It had a sensitivity of 23.45 nm/RIU, which is more sensitive than conventional refractive index sensor with LPG. The advantages of this sensor are the structural simplicity, ease of use, and its high sensitivity. As particle size increases, the wavelength of surface plasmon resonance related absorption shifts to longer, redder wavelengths. The surface plasmon resonance can be tuned by varying the size or shape of the nanoparticles, leading to particles with tailored optical properties for different applications. Surface plasmon resonance is an optical technique utilized for detecting molecular interactions. Binding of a mobile molecule (analytes) to a molecule

immobilized on a thin metal film (ligand) changes the refractive index of the film. An SPR fiber sensor with a fiber Bragg grating (FBG) for SPP excitation was described by Nemova and Kashyap [30]. If an FBG is used, then a very special fiber design is required to couple to SPR in a metal layer at the cladding surface since FBGs do not readily couple the core mode to the cladding modes. An SPR sensor using FBG was also proposed recently, in which hollow core (HC) fibers were adopted [31]. Other types of gratings have also been investigated, including tilted fiber gratings [32] and metallic Bragg gratings [33]. Both gratings show multiple peaks in the transmission spectrum of the SPR fiber sensor so that it is difficult to set the reference wavelength dip. However, the devices show sharp resonance dips and a good value for SNR. These grating- employed SPR fiber sensors show a slightly decreased sensitivity. ($10^2 \sim 10^3$ nm/RIU)

Compared to typical SPR fiber sensors. To couple light from the core mode to various cladding modes, other methods of fiber modifications have also been investigated. One involved the use of a cascaded side-polished fiber, intended to enhance the SPR effect, as shown in Fig. 8(b). The TM mode of guided wave in the fiber that enters the first SPR sensing region is rapidly exhausted, and half of the TE modes are coupled to TM modes in the coupling region

between the two sensing regions. More TM mode light is then delivered to the second sensing region and exhausted again. Results in a better resonance dip in transmission spectrum [34]. The sensitivity of a sensor can be improved by using two light-emitting diodes. Measurement of the difference in reflectance at. This much two wavelengths improve the sensitivity almost two fold, 5.2×10^{-4} RIU, as shown in Table 4 [35-36]. The reflection type sensor with a metal-coated fiber tip can also be modified to enhance the sensitivity. Fabricated submicron periodicity on gold-coated flat or the angled tip of fibers by focused ion beam milling in 2010. Many authors have proposed the design of PCF-based SPR sensors, which is based on the coupling of a leaky core mode to the SPP mode along a metalized fiber micro-structure. Numerically analyzed an SPR sensor based on a three-hole microstructured optical fiber with a gold layer deposited on the holes, as shown in Fig. 8(d). That numerical result indicates that very small optical loss and the sensing resolution of 10^{-4} RIU could be obtained. Prior to this the concept of a micro-structured optical fiber based SPR sensor with optimized micro-fluidics, which has a sensitivity of 10^{-4} RIU, which leads to a 1% change in the intensity of the transmitted light. Many types of SPR sensors with PCFs have also been proposed [37].

MICRO- OR NANO-STRUCTURED OPTICAL FIBER SENSORS

Characteristics of micro- or nano-structured optical fibers

Micro or nano-structured optical fibers cover a wide range of optical fibers, including PCFs and

some fibers with nano-structures at the end or side of optical fibers. With regard to PCFs, cording to the cross-sectional distribution of the dielectric function, PCFs can be categorized as follows: photonic-band gap fibers (PCF that utilizes the photonic bandgap and the defect mode), holey fibers (PCF with air holes along the axis of light propagation), hole-assisted fibers (PCF consisting of a conventional higher-index core with air holes), and Bragg fibers (photonic-bandgap fiber with concentric rings of different refractive indexes). The PCF has a periodic dielectric structure whose periodicity is on the order of a wavelength, giving rise to the photonic bandgap. The incident light whose wavelength lies within the photonic bandgap cannot propagate through the photonic crystal region and the transmission spectrum exhibits a wide bandgap. By locally breaking the period at the core, one can introduce a photonic defect mode within the bandgap and, as a result, the transmission spectrum has a relatively sharp transmission peak. The spectral position of the center of the transmission peak is highly sensitive to changes in the local environmental conditions. If liquid or gas molecules become bound to the defect, the local environmental condition, such as the refractive index, changes. Hence, it can be used as the sensing transduction signal. Because the light confinement provided by the photonic bandgap is very strong and because it is possible to easily adjust the defect mode wavelength across the photonic bandgap by finely tuning the structural parameters, PCF sensors have received huge attention since the first demonstration of the detection of a refractive index change in waveguide configurations.

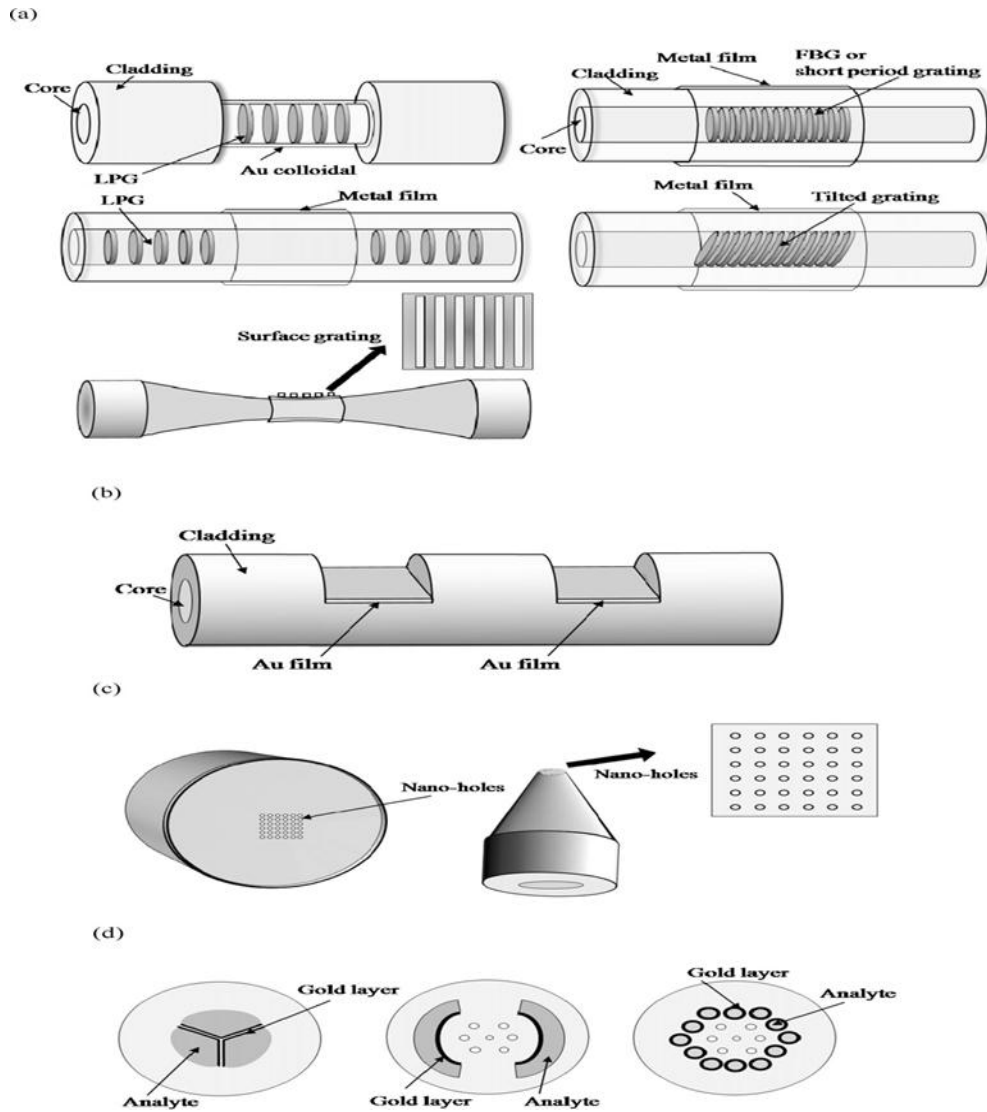


Fig. 8. Examples of SPR fiber sensors (a) with a long period grating (LPG), a short period grating (or fiber Bragg grating (FBG)), LPG pair, tilted grating, and metal surface grating, (b) with a

cascaded sensing region, (c) with nano-holes on a fiber tip that is flat or angled, and (d) with photonic crystal fibers.

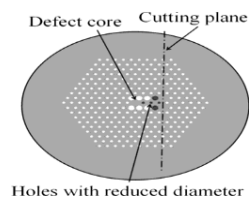


Fig. 9. Side-polished micro-structured optical fiber with small-diameter halls near the cutting plane

Performance of structured optical fiber sensors and other recent novel structures

To enhance interaction between guided lights and external materials, the fiber cladding can be partially removed by polishing to form a D-shape fiber to expose evanescent fields to the external materials. Numerous reports have appeared on the fabrication of and applications of the D-shape fiber [38]. Gaston et al. have devised temperature, relative humidity (RH), and pH sensors by using side-polished single mode fibers [39]. These sensors featured a temperature sensitivity of 8 dB/°C, a humidity sensitivity of 0.5 dB, and a change in the output power in 15 dB in the range from 2 to 11 pH. It was also proposed that an overlay of a porous TiO₂ coating deposited on the D-shape fiber can be used to improve RH sensitivity in low RH regime [40]. Chandani and Jaeger proposed a temperature sensor by etching a D-shape fiber in dilute hydrofluoric acid (HF), which features longer interaction lengths with a constant distance between the core edge and the flat surface. In particular, Franco et al. adapted the conventional concept of side-polishing to a micro-structured optical fiber (MOF) [41]. By reducing the diameters of the holes near the cutting plane (Fig. 9), the coupling of the evanescent field to the

external medium can be increased, giving rise to an enhanced sensitivity to changes in the external medium. It turned out that optimization of the geometrical configurations gives a wide operational temperature range of

$$\Delta T \cong 185^\circ\text{C}.$$

The sensitivity of between ~ 0.1 and ~ 0.38 dB/°C was obtained.

The HC-PCF sensor is composed of a hollow core and cladding holes. Either, or both, is filled with a measure and such as a liquid or gas, so that the interaction between the propagating light and the measure and results in change in the transmission properties. An important feature of the HC-PCF sensor is that it requires a small sample volume, compared to the D-shape MOF sensor owing to the longer interaction length and the high confinement of the guided mode. However, there are issues to be solved, in that the selective filling of the measure and is somewhat difficult and a preparation time is required. Cox et al. proposed a liquid-filled HC micro-structured polymer optical fiber (mPOF) [42]. It was shown that the HC-mPOF, when filled with a chiral solution, can be used for chemical sensing. Shi et al. described a FabryPerot type single point strain sensor with HC-PCF [43].

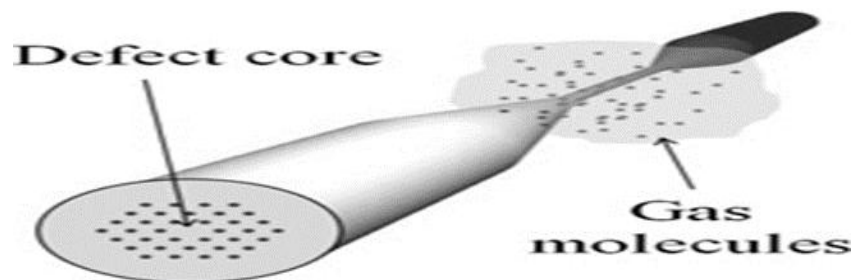


Fig.10. Photonic crystal fiber micro-taper structure for use in gas sensing.

In addition, by adapting FabryPerot interferometry (FPI) to HC-PCF, they proposed an HC-PCF-FPI strain sensor that has superb multiplexing capability, a wide free-spectral range (infinitesimal to more than 1200 nm), and temperature and bend independence [44]. It also features a high resolution and simple demodulation process. It was demonstrated that HC-PCF can be used for the detection of single-stranded deoxyribonucleic acid (SS-DNA) [45]. If the DNA

molecules in the aqueous solution form a 20 nm-thick surface inside the all-silica micro-structured HC Bragg fiber, the Bragg fiber confinement loss (CL) properties are changed. A finite element method (FEM) simulation showed that the DNA hybridization in the hole leads to a 100 nm-shift and 3 dB-increase in the CL minimum value. The MOF with an HC filled with liquids or a gas has also attracted considerable interest, due to its high Raman signal intensities. Since air-holes that

surround the HC reduce the effective refractive index of the cladding, liquids or a gas with a much lower refractive index can be applied to the structure [46]. That liquid-core air-cladding MOF provides a method for determining ethanol concentration by measuring the Raman spectrum of the liquid, after excitation by a frequency-doubled continuous-wave Nd: YAG laser [47]. To establish stable optical and liquid connections and to prevent the liquid from filling in the surrounding air-holes, the fiber ends of the HC-MOF are spliced to input and output MMFs. Experimental results for a set of ternary ethanol-sucrose solutions with known concentrations were in good agreement with the expected concentration with uncertainty ± 0.1 weight percentages.

The high-birefringence (Hi-Bi) PCF in a loop configuration has also attracted considerable interest [48]. Proposed a temperature-independent strain sensor in a loop mirror, in which two counter propagating beams from a 3 dB splitter experience different velocities due to strain-dependent birefringence. A simultaneous temperature and strain fiber sensor comprised of two types of Hi-Bi fibers with different responses to temperature and strain were devised [49]. It was also demonstrated that, by breaking the symmetry in the Hi-Bi PCF

inserted into the Sagnac interferometer, it can be used as curvature sensor [50]. This micro-structured asymmetric PCF is composed of two regions: one region with small diameter holes and the other with large diameter holes. The data show that the proposed sensor is not sensitive to longitudinal strain or temperature variation due to the characteristics of the pure silica and the group birefringence-based measurement technique used.

PCF fiber sensors with tapered or chirped structures have also been widely studied. A PCF micro-taper that supports two selective higher-order modes for use as a gas sensor has been proposed (Fig. 10) [51]. After tapering a PCF with three rings of air holes down to $3.5 \mu\text{m}$, they found that there can only be two higher-order modes (HE₀₅ and HE₀₆). It was shown that the difference between the propagation constants of the two modes was quite large and, because of this, the period of the interference pattern was short. The presence of gas molecules in the tapered region gives rise to a change in the surface refractive index, leading to a shift in the interference pattern. An advantage for the proposed device is that there is no need to fill the air-holes in the PCFs with the gas measure and, which usually requires lengthy preparation time.

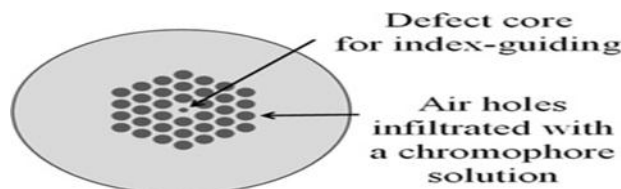


Fig. 11. Evanescent field absorption sensor based on a pure-silica defected-core photonic crystal fiber.

The structured chirped FBGs, consisting of a chirped FBG and single or multiple defects [52]. The core propagation properties can be modified by changing the surrounding refractive index of the thinned region in the cladding layer, leading to a change in the reflectivity spectrum. Although the sensitivity would be expected to be 10–5 and 10–4 RIU for a surrounding refractive index of around 1.50 and 1.30, respectively, which are lower than those of other methods, the proposed structure features low cost interrogations and the ability of using multi-point refractometers for chemical sensing. An evanescent field absorption sensor

based on a pure-silica defected-core PCF has been demonstrated experimentally (Fig. 11) [53]. Contrary to evanescent field spectroscopy in conventional fibers, the defected-core PCF exhibits higher sensitivity due to the fact that the evanescent field overlap can be significantly enhanced by the large contact area between air-holes and infiltrations such as liquids and gas. As an absorber, various concentrations of cobalt chloride (CoCl₂), ranging from 0.001 ~ 0.70 Mol were injected into the fiber samples. The transmission spectra reveal that the absorption increases with increasing concentrations of CoCl₂

and the longitudinal detection has a higher sensitivity, up to 70 times compared to that found for perpendicular detection. It is known that the fundamental absorption peak of a gas typically lies in the mid-IR regime ($3\ \mu\text{m}$), in which most optical fibers do not support guided modes. Thus, higher absorption modes have been used to interact with light in the near IR regime, resulting in the requirement for a long interaction length and the need for highly sensitive techniques. Gayraud et al. have devised a novel design of PBFs for methane sensing at $3.0\ \mu\text{m}$ [54]. Using a femtosecond optical parametric oscillator as an optical source and Fourier transform infrared (FTIR) spectroscopy [55], they reported that 1000 ppm of methane can be measured and predicted that the sensitivity could be improved so as to measure concentrations up to 50 ppm with the use of the recently emerging new light sources.

LPGs engraved in a PCF allow modal coupling between the cores and cladding modes. This gives rise to a high degree of sensitivity for the

resonance wavelengths, which leads to changes in the refractive index of materials in the cladding air channels. Using numerical techniques, Zhu et al. investigated the refractive index sensitivity of endless single mode PCF-LPGs [56]. Their results showed that, owing to the efficient overlap of the evanescent field with the measure and, a very high sensitivity of 10^{-8} RIU was possible. Meanwhile, developments in the area of femtosecond laser processing techniques have been used to fabricate micro-fluidic devices on various Structures [57]. In particular, micro-fluidic channels written in a step-index optical fiber can affect the scattering properties of the core-guided light, rather than the evanescent field in the cladding. Inspired by this feature. Proposed a micro-slit-based refractive index sensor, which takes advantage of the fact that, the change in the refractive index in the micro-slit in a step-index fiber influences the propagation properties through the fiber [58]. It was shown that optimization processes in shape or dimension can be used for a particular application.

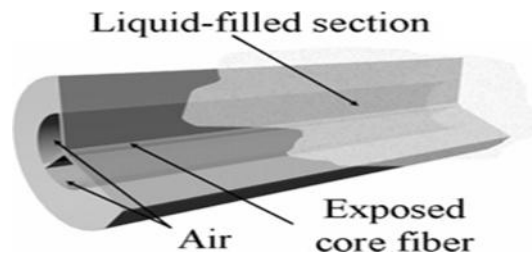


Fig. 12. Wagon wheel fiber after removing one-third of the air-holes.

The quantitative broadband fiber sensor using evanescent field sensing in the cladding holes of an air-suspended solid-core PCF [59]. The results showed that the sensitivity could be enhanced up to three orders of magnitude compared to standard cuvettes for both liquid and gas sensing. Absorption spectra, obtained using various concentrations of aqueous NiCl_2 solutions were in good agreement with the reference spectrum, whereas the sample volume was reduced by three orders of magnitude. There has also been another approach to enhance overlap of the guided mode into the sensing region [60]. By removing one-third of the air-holes in the cladding of a wagon wheel fiber (Fig. 12), direct access between the nano-wire core suspended in the air-holes and the

sensing material can be affected. A numerical investigation revealed that the proposed exposed-core MOF exhibits an enhanced fluorescence capture efficiency of up to 35%.

CONCLUSION

This paper mainly focused on study the functionality of various elements like Optical fiber SPR sensors and PCF sensors. Fiber-optic SPR sensors have diverse structures that include D-shaped, cladding-off, end-reflection, angled fiber tip fiber structures. The typically used metals are gold and silver. Metal thickness is an important parameter in determining sensor characteristics. Over layers can be used on top of the metal to

further appropriately adjust the sensor measurement characteristics. Many novel SPR fiber sensors using fiber gratings or adopting PCF concepts have been proposed recently. Although the basic principle of an SPR sensor is simple, its numerical analysis is not straight-forward, especially for structures lacking in cylindrical symmetry. A numerical analysis should be considered to be only a guideline in fiber-optic SPR sensor design. Real fabricated sensors show different characteristics because of non-ideal parameters. Some data on sensitivities and detection ranges of refractive index of SPR fiber

sensors can be found in Tables 2 and 4. The PCF sensor constitutes a subject of considerable interest as well. Various categories of PCF sensors exist, in which photonic-band gap fibers, holey fibers, hole-assisted fibers and Bragg fibers are used. Two major application fields of these sensors are as gas sensors and as bio-sensors. The micro- and nano-structured fiber sensors overviewed in this paper would be expected to attract much interest for research and development for some years to come, due to, not only their advantages of high sensitivity, small sensor head footprint and flexibility of optical fibers.

REFERENCES

- [1]. B. Lee, Review of the present status of optical fiber sensors, *Opt. Fiber Technology*, 9 (2), 2003, 57–79.
- [2]. Sharma, R. Jha, B.D. Gupta, Fiber-optic sensors based on surface plasmon resonance: A comprehensive review, *IEEE Sensors J.*, 7 (8), 2007, 1118–1129.
- [3]. F. Villuendas, J. Pelayo, Optical fibre device for chemical sensing based on surface plasmon excitation, *Sens. Actuators A*, 23, 1990, 1142–1145.
- [4]. L. de Maria, M. Martinelli, G. Vegetti, Fiber-optic sensor based on surface plasmon interrogation, *Sens. Actuators B*, 12, 1993, 221–223.
- [5]. S.A. Maier, *Plasmonics – Fundamentals and Applications*, Springer, New York, 2007.
- [6]. E. Kretschmann, H. Raether, Radiative decay of nonradiative surface plasmons excited by light, *Z. Naturforsch. Teil A* 23, 1968, 2135–2136.
- [7]. S. Kim, H. Kim, Y. Lim, B. Lee, Off-axis directional beaming of optical field diffracted by a single sub-wavelength metal slit with asymmetric dielectric surface gratings, *Appl. Phys. Lett.*, 90(5), 2007, 051113.
- [8]. M.D. Malinsky, K.L. Kelly, G.C. Schatz, R.P. van Duyne, Chain length dependence and sensing capabilities of the localized surface plasmon resonance of silver nanoparticles chemically modified with alkanethiol self-assembled monolayers, *J. Am. Chem. Soc.*, 123, 2001, 1471–1482.
- [9]. A.K. Sharma, Rajan, B.D. Gupta, Influence of dopants on the performance of a fiber optic surface plasmon resonance sensor, *Opt. Commun.*, 274, 2007, 320–326.
- [10]. J. Homola, Optical fiber sensor based on surface plasmon excitation, *Sens. Actuators B* 29 (1995) 401–405.
- [11]. A.K. Sharma, B.D. Gupta, Comparison of performance parameters of conventional and nano-plasmonic fiber optic sensors, *Plasmonics* 2 (2007) 51–54.
- [12]. A.K. Sharma, B.D. Gupta, Fibre-optic sensor based on surface plasmon resonance with Ag–Au alloy nanoparticle films, *Nanotechnology.*, 17 (1), 2006, 124–131.
- [13]. R.K. Verma, A.K. Sharma, B.D. Gupta, Surface plasmon resonance based tapered fiber optic sensor with different taper profiles, *Opt. Commun.* 281, 2008, 1486–1491.
- [14]. S.-F. Wang, M.-H. Chiu, J.-C. Hsu, R.-S. Chang, F.-T. Wang, Theoretical analysis and experimental evaluation of D-type optical fiber sensor with a thin gold film, *Opt. Commun.*, 253, 2005, 283–289.
- [15]. H. Suzuki, M. Sugimoto, Y. Matsui, J. Kondoh, Effects of gold film thickness on spectrum profile and sensitivity of a multimode-optical-fiber SPR sensor, *Sens. Actuators B*, 132, 2008, 26–33.
- [16]. Z. Zhang, P. Zhao, F. Sun, G. Xiao, Y. Wu, Self-referencing in optical-fiber surface plasmon resonance sensors, *IEEE Photon. Technol. Lett.* 19(24), 2008, 1958–1960.

- [17]. J. Villatoro, D. Monzón-Hernández, E. Mejia, Fabrication and modeling of uniform-waist single-mode tapered optical fiber sensors, *Appl. Opt.* 42(13), 2003, 2278–2283.
- [18]. D.J. Pena, M.J. Natan, Surface plasmon resonance of colloidal Au-modified gold films, *Sens. Actuators B*, 54, 1999, 118–124.
- [19]. Surface-plasmon resonance sensor with bimetallic layers, *Opt. Commun.*, 245, 2005, 159–169.
- [20]. C.-S. Cheng, Y.-Q. Chen, C.-J. Lu, Organic vapour sensing using localized surface plasmon resonance spectrum of metallic nanoparticles self-assembled mono-layer, *Talanta*, 73, 2007, 358–365.
- [21]. S. Link, Z.L. Wang, M.A. El-Sayed, Alloy formation of gold-silver nanoparticles and the dependence of the plasmon absorption on their composition, *J. Phys. Chem. B*, 103, 1999, 3529–3533.
- [22]. Diez, M.V. Andres, J.L. Cruz, In-line fiber-optic sensors based on the excitation of surface plasma modes in metal-coated tapered fibers, *Sens. Actuators B*, 73, 2001, 95–99.
- [23]. Y.-C. Kim, S. Banerji, J.-F. Masson, W. Peng, K.S. Booksh, Fiber-optic surface plasmon resonance for vapor phase analyses, *Analyst* 130, 2005, 838–843.
- [24]. S.D. Soelberg, T. Chinowsky, G. Geiss, G.G. Spinelli, R. Stevens, S. Near, P. Kauffman, S. Yee, C.E. Furlong, A portable surface plasmon resonance sensor system for real-time monitoring of small to large analytes, *J. Ind. Microbiol. Biotechnology*, 32, 2005, 669–674.
- [25]. J. Ctyroky, F. Abdelmalek, W. Ecke, K. Usbeck, Modelling of the surface plasmon resonance waveguide sensor with Bragg grating, *Opt. Quantum Electron.* 31, 1999, 927–941.
- [26]. J. Ctyroky, J. Homola, M. Skalsky, Modelling of surface plasmon resonance waveguide sensor by complex mode expansion and propagation method, *Opt. Quant. Electron.* 29, 1997, 301–311.
- [27]. W. Bin, W.Q. Kang, High sensitivity transmission-type SPR sensor by using metallic-dielectric mixed gratings, *Chin. Phys. Lett.*, 25(5), 2008, 1668–1671.
- [28]. D. Zhang, P. Wang, X. Jiao, G. Yuan, J. Zhang, C. Chen, H. Ming, R. Rao, Investigation of the sensitivity of H-shaped nano-grating surface plasmon resonance biosensors using rigorous coupled wave analysis, *Appl. Phys. A*, 89, 2007, 55–58.
- [29]. Y.-J. He, Y.-L. Lo, J.-F. Huang, Optical-fiber surface-plasmon-resonance sensor employing long period fiber gratings in multiplexing, *J. Opt. Soc. Am. B*, 23(5), 2006, 801–811.
- [30]. J.-L. Tang, S.-F. Cheng, W.-T. Hsu, T.-Y. Chiang, L.-K. Chau, Fiber-optic biochemical sensing with a colloidal gold-modified long period fiber grating, *Sens. Actuators B*, 119, 2006, 105–109.
- [31]. G. Nemova, R. Kashyap, Fiber-Bragg-grating-assisted surface plasmon-polariton sensor, *Opt. Lett.*, 31(14), 2006, 2118–2120.
- [32]. G. Nemova, R. Kashyap, Modeling of plasmon-polariton refractive-index hollow core fiber sensors assisted by a fiber Bragg grating, *J. Lightwave Technol.* 24(10), 2006, 3789–3796.
- [33]. T. Allsop, R. Neal, S. Rehman, D.J. Webb, D. Mapps, I. Bennion, Characterization of infrared surface plasmon resonances generated from a fiber-optical sensor utilizing tilted Bragg gratings, *J. Opt. Soc. Am. B*, 25(4), 2008, 481–490.
- [34]. W. Ding, S.R. Andrews, T.A. Birks, S.A. Maier, Modal coupling in fiber tapers decorated with metallic surface gratings, *Opt. Lett.* 31(17), 2006, 2556–2558.
- [35]. Y.-C. Lin, W.-H. Tsai, Y.-C. Taso, J.-K. Tai, An enhanced optical multimode fiber sensor based on surface plasmon resonance with cascaded structure, *IEEE Photon. Technol. Lett.*, 20(15), 2008, 1287–1289.
- [36]. H. Suzuki, M. Sugimoto, Y. Matsui, J. Kondoh, Fundamental characteristics of a dual-colour fibre optic SPR sensor, *Meas. Sci. Technol.*, 17, 2006, 1547–1552.
- A. Dhawan, M.D. Gerhold, J.F. Muth, Plasmonic structures based on sub wavelength apertures for chemical and biological sensing applications, *IEEE Sensors J.* 8(6), 2008, 942–950.
- [37]. Hassani, B. Gauvreau, M.F. Fehri, A. Kabashin, M. S korobogatiy, Photonic crystal fiber and waveguide-based surface plasmon resonance sensors for application in the visible and near-IR, *Electromagnetics* 28, 2008, 198–213.
- [38]. S.-M. Tseng, C.-L. Chen, Side-polished fibers, *Appl. Opt.* 31(18), 1992, 3438–3447.

- A. Gaston, I. Lozano, F. Perez, F. Auza, J. Sevilla, Evanescent wave optical-fiber sensing (temperature, relative humidity, and pH sensors), *IEEE Sensors J.*, 3(6), 2003, 806–811.
- [39]. Alvarez-Herrero, H. Guerrero, D. Levy, High-sensitivity sensor of low relative humidity based on overlay on side-polished fibers, *IEEE Sensors J.*, 4(1), 2004, 52–56.
- [40]. M.A.R. Franco, V.A. Serrão, F. Sircilli, Side-polished microstructured optical fiber for temperature sensor application, *IEEE Photon. Technol. Lett.*, 19(21), 2007, 1738–1740.
- [41]. F.M. Cox, A. Argyros, M.C.J. Large, Liquid-filled hollow core microstructured polymer optical fiber, *Opt. Express* 14(9), 2006, 4135–4140.
- [42]. Q. Shi, F. Lu, Z. Wang, L. Jin, J.J. Hu, Z. Liu, G. Kai, X. Dong, Environmentally stable Fabry–Pérot-type strain sensor based on hollow-core photonic bandgap fiber, *IEEE Photon. Technol. Lett.* 20(4), 2008, 237–239.
- [43]. Q. Shi, F. Lu, Z. Wang, L. Jin, Y. Li, Z. Liu, G. Kai, X. Dong, Environmentally stable Fabry–Pérot-type strain sensor based on hollow-core photonic bandgap fiber, *IEEE Photon. Technol. Lett.* 20(15), 2008, 1329–2391331.
- [44]. D. Passaro, M. Foroni, F. Poli, A. Cucinotta, S. Selleri, J. Lægsgaard, A.O. Bjarklev, All-silica hollow-core microstructured Bragg fibers for biosensor application, *IEEE Sensors J.*, 8(7), 2008, 1280–1286.
- [45]. S. Yiou, P. Delaye, A. Rouvie, J. Chinaud, R. Frey, G. Roosen, P. Viale, S. Février, P. Roy, J.-L. Auguste, J.-M. Blondy, Stimulated Raman scattering in an ethanol core microstructured optical fiber, *Opt. Express.*, 13(12), 2005, 4786–4791.
- [46]. D. Monzón-Hernández, V.P. Minkovich, J. Villatoro, M.P. Kreuzer, G. Badenes, Photonic crystal fiber microtaper supporting two selective higher-order modes with high sensitivity to gas molecules, *Appl. Phys. Lett.*, 8(7), 2008, 1250-1255
- [47]. Y. Liu, B. Liu, X. Feng, W. Zhang, G. Zhou, S. Yuan, G. Kai, X. Dong, High-birefringence fiber loop mirrors and their applications as sensors, *Appl. Opt.*, 44(12), 2005, 2382–2390.
- [48]. S. Venkateswa Rao Simultaneous temperature and strain measurement using two types of High-birefringence fibers in Sagnac loop mirror, 2007, 2027-2029
- [49]. O. Frazão, J.M. Baptista, J.L. Santos, P. Roy, Curvature sensor using a highly birefringent photonic crystal fiber with two asymmetric hole regions in a Sagnac interferometer, *Appl. Opt.*, 47(13), 2008, 2520–2523.
- [50]. D. Monzón-Hernández, V.P. Minkovich, J. Villatoro, M.P. Kreuzer, G. Badenes, Photonic crystal fiber microtaper supporting two selective higher-order modes with high sensitivity to gas molecules, *Appl. Phys. Lett.*, 93, 2008, 081106.
- [51]. M. Pisco, A. Iadicco, S. Campopiano, A. Cutolo, A. Cusano, Structured chirped fiber Bragg gratings, *IEEE J. Lightwave Technol.*, 26(12), 2008, 1613–1625.
- [52]. X. Yu, Y. Sun, G.B. Ren, P. Shum, N.Q. Ngo, Y.C. Kwok, Evanescent field absorption sensor using a pure-silica defected-core photonic crystal fiber, *IEEE Photon. Technol. Lett.*, 20(5), 2008, 336–338.
- [53]. N. Gayraud, L.W. Kornaszewski, J.M. Stone, J.C. Knight, D.T. Reid, D.P. Hand,
- [54]. W.N. MacPherson, Mid-infrared gas sensing using a photonic bandgap fiber, *Appl. Opt.*, 47(9), 2008, 1269–1277.
- [55]. K.A. Tillman, R.R.J. Maier, D.T. Reid, E.D. McNaghten, Mid-infrared absorption spectroscopy of methane using a broadband femtosecond optical parametric oscillator based on a periodically poled lithium niobate, *J. Opt. A Pure Appl. Opt.*, 7, 2005, S408–S414.
- [56]. Y. Zhu, Z. He, J. Kanka, H. Du, Numerical analysis of refractive index sensitivity of long-period gratings in photonic crystal fiber, *Sens. Actuators B.*, 129, 2008, 99–105.
- [57]. A.v. Brakel, C. Grivas, M.N. Petrovich, D.J. Richardson, Micro-channels machined in microstructured optical fibers by femtosecond laser, *Opt. Ex-press.*, 15(14), 2007, 8731–8736.
- [58]. J. Petrovic, Y. Lai, I. Bennion, Numerical and experimental study of microfluidic devices in step-index optical fibers, *Appl. Opt.*, 47(10), 2008, 1410–1416.

- [59]. T.G. Euser, J.S.Y. Chen, M. Scharrer, P.St.J. Russell, N.J. Farrer, P.J. Sadler, Quantitative broadband chemical sensing in air-suspended solid-core fibers, *J. Appl. Phys.*, 103, 2008, 103108.
- [60]. S.C. Warren-Smith, S.V. Afshar, T.M. Monro, Theoretical study of liquid-immersed exposed-core microstructured optical fibers for sensing, *Opt. Express.*, 16(12), 2008, 9034–9045.